



CHORUS

This is the accepted manuscript made available via CHORUS. The article has been published as:

Enhancement of Thermal Conductance at Metal-Dielectric Interfaces Using Subnanometer Metal Adhesion Layers

Minyoung Jeong, Justin P. Freedman, Hongliang Joe Liang, Cheng-Ming Chow, Vincent M. Sokalski, James A. Bain, and Jonathan A. Malen

Phys. Rev. Applied **5**, 014009 — Published 26 January 2016

DOI: [10.1103/PhysRevApplied.5.014009](https://doi.org/10.1103/PhysRevApplied.5.014009)

Enhancement of thermal conductance at metal-dielectric interfaces using sub-nanometer metal adhesion layers

Minyoung Jeong,¹ Justin P. Freedman,¹ Hongliang Joe Liang,² Cheng-Ming Chow,² Vincent M. Sokalski,¹ James A. Bain,² and Jonathan A. Malen^{1,3,*}

¹*Department of Materials Science and Engineering,
Carnegie Mellon University, Pittsburgh, Pennsylvania, 15213*

²*Department of Electrical and Computer Engineering,
Carnegie Mellon University, Pittsburgh, Pennsylvania, 15213*

³*Department of Mechanical Engineering,
Carnegie Mellon University, Pittsburgh, Pennsylvania, 15213*

(Dated: December 23, 2015)

Abstract

We show that the use of sub-nm adhesion layers significantly enhances the thermal interface conductance at metal-dielectric interfaces. A metal-dielectric interface between Au and sapphire (Al_2O_3) was considered using Cu (low optical loss) and Cr (high optical loss) as adhesion layers. To enable high throughput measurements each adhesion layer was deposited as a wedge such that a continuous range of thickness could be sampled. Our measurements of thermal interface conductance at the metal- Al_2O_3 interface made using frequency domain thermoreflectance show that a 1 nm thick adhesion layer of Cu or Cr is sufficient to enhance the thermal interface conductance by more than a factor of 2 or 4, respectively, relative to the pure Au- Al_2O_3 interface. The enhancement agrees with the Diffuse Mismatch Model-based predictions of accumulated thermal conductance versus adhesion layer thickness assuming that it contributes phonons with wavelengths less than its adhesion layer thickness, while those with longer wavelengths transmit directly from the Au.

I. INTRODUCTION

Recent advances in modern micro- and nanotechnologies have opened new possibilities for smaller yet faster and more efficient electronic and optoelectronic devices. Optimal performance of these small devices requires effective thermal management, even at the level of interfaces due to the increased surface to volume ratio that accompanies reduced dimensions.¹⁻⁴ For example, heat-assisted magnetic recording (HAMR) is a promising option for the next generation of data storage in which interfacial thermal properties play a critical role. In this technology, a near-field transducer (NFT) heats the magnetic media in a localized region (~ 50 nm) through the delivery of electromagnetic radiation focused by a gold (Au)-dielectric plasmonic interface.⁵⁻⁷ Heat generated due to parasitic losses in the Au itself is dissipated to the dielectric and results in peak NFT temperatures hundreds of degrees above the ambient temperature.⁵ High thermal conductivity dielectrics such as aluminum nitride (AlN) or sapphire (Al_2O_3) would be preferred, therein making their interface with Au the clear bottleneck to heat dissipation.

The rate of heat transfer across the interface is described in terms of the thermal interface conductance (G), defined as $q''/\Delta T$, where q'' is the heat flux across an interface, and ΔT is the temperature difference across the interface.⁸ The reported values of G for the Au/ Al_2O_3 interface range from $22 \text{ MW m}^{-2}\text{K}^{-1}$ to $66 \text{ MW m}^{-2}\text{K}^{-1}$ at a temperature of 300 K,^{9,10} which is low compared to other metal-dielectric interfaces^{10,11}. The Kapitza length, defined as κ/G , represents the thickness of material with the thermal conductivity κ that has equivalent resistance to the interface. Taking κ of Al_2O_3 as $38 \text{ Wm}^{-1} \text{K}^{-1}$,¹² and using the aforementioned G , the Kapitza length of Al_2O_3 ranges from 575 nm to $1.72 \mu\text{m}$, which is far larger than typical NFT dimensions or the distance within the dielectric over which the temperature around the NFT drops.⁵

Electrons are the main heat carriers in metals, while phonons are the main heat carriers in crystalline dielectrics. It has been proposed that electrons first transfer their energy to phonons in the metal with an equivalent conductance of G_{e-p} , and the phonons in the metal then transmit through the interface into the dielectric with G_p . Because these processes represent thermal resistances in series, G becomes $(G_{e-p} G_p)/(G_{e-p} + G_p)$.¹³⁻²⁰ The ratio of $\frac{G_{e-p}}{G_p}$ in the Au- Al_2O_3 interface is nearly 5.^{13,21} Because G_{e-p} is larger as shown by Wang et al.,²² the G_p term becomes a bottle neck in the overall G . Notably, Wang et al. showed that temperature

dependent measurements of the electron-phonon coupling constant in thin films agree with Kagnov's classical theory for bulk materials.^{22,23} Thus, understanding and enhancing phonon transport across the interface is essential.

One possible approach to enhance G is to insert adhesion layers between the two materials.²⁴ Good candidate materials should possess similar Debye temperatures to the substrate^{10,11,25}, with strong adhesion, and affordable costs. For plasmonic technologies the optical properties of an adhesion layer, which will impact the plasmonic properties of a Au-dielectric interface are also critically important. Ideally the adhesion layer thickness would be minimized to maintain the plasmonic properties, but it is not precisely known how thick an adhesion layer is required to improve thermal performance.

In this study, we seek to answer how thick an adhesion layer is required to provide thermal benefits at a plasmonic interface. Frequency domain thermoreflectance (FDTR), a non-contact optical technique, was used to experimentally measure G across a Au- Al_2O_3 interface as a function of adhesion layer thickness. In order to sample fine increments of thickness the adhesion layers were deposited in a wedge shape on Al_2O_3 wafers such that a continuous taper from 0 to ~ 7 nm exists. Cu and Cr adhesion layers were considered because they represent low and high optical loss metals in the near-infrared (IR), yet both have higher Debye temperatures than Au. The experimentally measured G values were then compared to Diffuse Mismatch Model (DMM)-based predictions to determine whether phonon alignment alone could account for observed enhancements of G in adhesion layers that are just 1 nm thick.

II. EXPERIMENT

Thin films were deposited on 3-inch Al_2O_3 c-plane (0001) wafers by DC magnetron sputtering from 5-inch targets in an argon atmosphere with a base pressure maintained at $< 2 \times 10^{-7}$ Torr. Substrates were cleaned with acetone in an ultrasonic bath for 10 minutes and then rinsed with isopropyl alcohol (IPA). Cr and Cu deposition rates were $0.67 \text{ \AA}/\text{sec}$ at 5 mTorr and $2.25 \text{ \AA}/\text{sec}$ at 2.5 mTorr, respectively.

Wedge films were prepared by moving the substrate into the target's deposition window at a controlled velocity before reversing direction so that the leading edge was exposed to the plasma longer than the trailing edge. This process resulted in a thickness gradient with a targeted range between 0 and 6-8 nm. A 70 nm Au transducer layer of uniform thickness was

deposited in a non-wedge shape on each of the adhesion layers without breaking vacuum as shown in Fig.1. Cu and Cr samples were fabricated additionally without Au for AFM analysis. AFM images taken at various positions on the wedge verify that the adhesion layers were deposited as continuous films without islanding. The spatially varying thickness of each adhesion layer and the Au layer were measured using x-ray reflectivity (XRR). The uncertainty in XRR data fitting of the adhesion layer thickness was ± 0.3 nm.²⁶

The thermal interface conductance values at the metal- Al_2O_3 interface were measured as a function of adhesion layer thickness by FDTR.²⁷⁻²⁹ In this technique an electrooptic modulator intensity modulates a 488 nm continuous wave (CW) pump laser over a range of frequencies (from 200 kHz to 10 MHz in this study). When the modulated pump beam is absorbed by the sample surface it periodically heats the sample at the pump beam modulation frequency. This periodic heating generates corresponding changes in temperature at the surface that have a phase lag relative to the heating that depends on G . This periodic temperature response is detected by a 532 nm CW probe laser beam that is co-aligned with the pump at the sample surface. The phase-lag data between the reflected pump and the probe beams at different positions on the substrate were obtained using a lock-in amplifier. A total of 40 data points were collected at each frequency and then fit to a widely-used analytical solution of the heat diffusion equation.³⁰ By fitting this model to G at each position on the wafer we extracted G at different adhesion layer thicknesses. The values and uncertainties in the fitting parameters are shown in Table 1.

Table I: Layer properties for FDTR analysis³¹⁻³³

Layer	Thickness (nm)	k ($\text{Wm}^{-1} \text{K}^{-1}$)	Heat Capacity ($\text{Jkg}^{-1} \text{K}^{-1}$)	Density (g/cm^3)
Au-layer	71 ± 2.0 (Cu sample)	146 ± 4.0 (Cu sample)	126 ± 3.0	19.3 ± 0.4
	70 ± 2.0 (Cr sample)	161 ± 5.0 (Cr sample)		
Cu-layer	Fig.1	146 ± 4.0	390 ± 5.0	9.0 ± 0.2
Cr-layer	Fig.1	161 ± 5.0	450 ± 10	7.2 ± 0.2
Al_2O_3 -substrate	500×10^3	38 ± 2.0	760 ± 50	4.0 ± 0.1

In modeling the system several parameters and assumptions were equivalently applied to

all data points. The Au thermal conductivity (k_{Au}) for each sample was calculated using the Wiedmann-Franz (WF) Law based on the electrical conductivity measured by a four point probe on a region of the sample without the adhesion layer. The Au was modeled as isothermal as Refs. 34,35 to mimic energy deposition at a finite depth and electron-phonon equilibration lengthscales of ~ 100 nm.²² To include this effect we reduced the Au thickness to 1 nm (from $\sim X$ nm), multiplied its heat capacity by X so the total heat capacity was unchanged, and multiplied its WF thermal conductivity by X so in-plane conduction was unchanged. The adhesion layer was modeled with the Au thermal conductivity. Since the adhesion layer is thinner than electron mean free paths, electron transport across the layer is ballistic and scattering is dominated by interfaces, such that suppression of its intrinsic thermal conductivity is inappropriate. Moreover, its equivalent thermal conductance ($k/\text{Thickness}$) based on bulk Cu or Cr properties is $> 10,000$ MW m²K⁻¹ (> 25 times our largest measured G values), even for the thickest layers, meaning that this assumption has little influence on the predicted G at the Al₂O₃ interface. Additionally, we have assumed an infinite thermal interface conductance between the Au layer and the adhesion layer. Typical metal-metal thermal interface conductances are an order of magnitude larger than metal-dielectric interfaces (e.g. ~ 3.5 GW m²K⁻¹ for the Au-Cu interface³⁶), making us insensitive to this value even if it varies with adhesion layer thickness. Each of the above assumptions may introduce small systematic shifts in the reported G , but their influence on the thickness dependent trends is negligible and not reflected in the uncertainty discussed below. Finally, we choose to report the composite G rather than separating the G_{e-p} and G_p components in what follows, since the electron-phonon coupling coefficient may be influenced by adhesion layer thickness. Based on the analysis in Ref. 15 with the reported properties of Cu and Cr³⁷⁻⁴¹ we estimate electron-phonon coupling conductances of 700 MW m⁻²K⁻¹ and 3,000 MW m⁻²K⁻¹.

The uncertainty in G , reported as errorbars in Fig. 1, results from propagation of the uncertainty in the input parameters through the fitting analysis.²⁸ The major sources of uncertainty were laser spot radius and Al₂O₃ thermal conductivity. The $1/e^2$ laser spot radius of 2.8 ± 0.1 μm was measured using the knife-edge technique. Al₂O₃ thermal conductivity of 38 ± 2 Wm⁻¹ K⁻¹ was used for all samples.¹² We quote an uncertainty in our sapphire conductivity in order to reflect the range of reported values in the literature, but the same number (38 Wm⁻¹ K⁻¹) was used in all of the analysis and this uncertainty does not affect our conclusions. For the spot size and range of frequencies used in this study non-diffusive effects are not ex-

pected in Al_2O_3 because 95% of its thermal conductivity results from phonons with mean free paths less than 1000 nm.⁴²

III. RESULTS AND DISCUSSION

The thicknesses of Cu and Cr adhesion layers measured by XRR on the Al_2O_3 substrate are shown in Fig. 1. The XRR measurements determined the Au layers to be 71 ± 2 nm and 70 ± 2 nm thick with maximum adhesion layer thicknesses of 7.3 ± 0.3 nm and 8.2 ± 0.3 nm at the Cu and Cr wedge edges. One of the XRR fits at an intermediate position on the Cu wedge is shown in the inset of Fig. 1. Positions on the substrate were measured in terms of the normal distance from the flat edge on the Al_2O_3 substrates. Non-linearity in the thickness gradients result from variation in the deposition rate across the target shutter opening. A third order polynomial fit ($R^2 > 0.99$) to the measured data was used to extract the adhesion layer thicknesses as a function of position on the substrate.

The thermal interface conductance of Cu and Cr samples are shown in Fig. 2(a) and (b) and exhibit an increasing trend as the layers become thicker. In the "non-wedge" region, where only the Au- Al_2O_3 interface is present, average G values of 70 ± 10 $\text{MW m}^{-2}\text{K}^{-1}$ and 60 ± 10 $\text{MW m}^{-2}\text{K}^{-1}$ for Cu and Cr samples were measured. This range agrees well with measurements of a Au- Al_2O_3 interface by Stoner and Maris.¹⁰ Furthermore, as presented in Fig. 2(b), we observed more than two and four fold enhancements of G for 1 nm Cu and

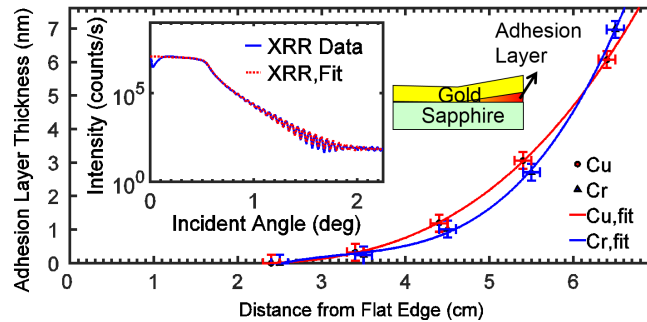


Figure 1: The wedge form of Cu and Cr adhesion layer thickness as a function of position on the substrate. Third order polynomial fits for both experimental data were added. The inset schematic shows the adhesion layer wedge. The inset plot shows XRR data and fits for a 1.20 nm thick position on the Cu wedge.

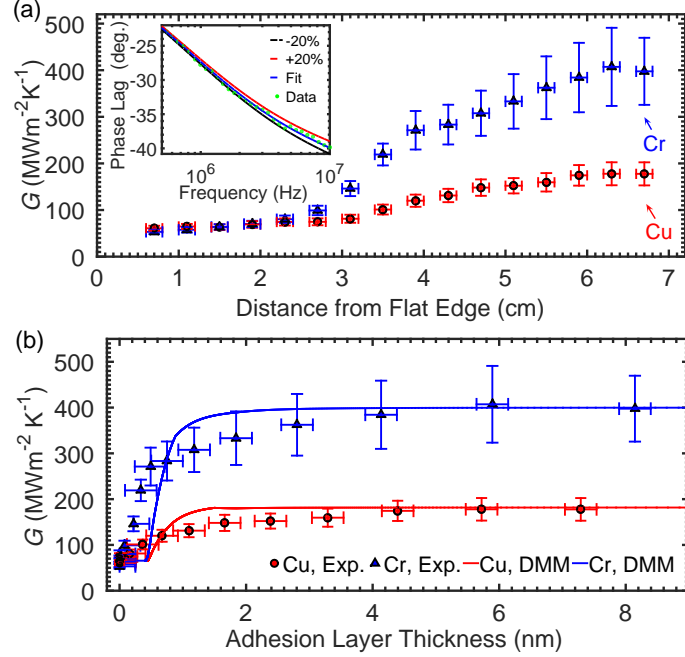


Figure 2: (a) Experimentally obtained G increases with an increasing adhesion layer thickness for both Cu and Cr. The Cr adhesion layer exhibited a greater increase in G than the Cu with both samples saturating beyond approximately 5 nm. The inset shows the sensitivity of fitting phase-lag data to $\pm 20\%$ of G for the Cr sample at a thickness of 1.10 nm.

(b) The experimental values were compared with DMM-based predictions of the accumulation functions of G in terms of Cu or Cr thickness.

Cr adhesion layers, respectively, between the Au and Al_2O_3 . The measured G saturated at $180 \pm 20 \text{ MW m}^{-2}\text{K}^{-1}$ and $390 \pm 70 \text{ MW m}^{-2}\text{K}^{-1}$, for Cu and Cr adhesion layers, once the layer thickness reached approximately 5 nm. Such significant enhancement cannot be attributed to an increase in G_{e-p} in Cu and Cr relative to Au, since this alone would result in a maximum increase of $\sim 20\%$ in G , assuming $G_{e-p}/G_p \cong 5$ in Au. This clearly shows that only a few angstroms of the adhesion layer are needed to significantly increase G . From a technological standpoint this is an important finding for HAMR and other plasmonic devices because thinner adhesion layers will minimize degradation of the optical performance at the plasmonic interface.

To better understand the enhancement in G we compare our measurements with the predictions of G_p based on the DMM.^{42,43} The DMM is more appropriate than the acoustic mis-

match model (AMM) at high temperatures, and as we quantify later the AMM severely overestimates our experimental data for the Au-Al₂O₃ interface.^{8,44} A general expression for G_p is,⁴⁵

$$G_p = \frac{1}{8\pi^2} \sum_j \int_{K_{j,1}} \hbar \omega_{j,1}(K_{j,1}) K_{j,1}^2 \zeta^{1-2} |v_{j,1}(K_{j,1})| \frac{\partial n_0}{\partial T} dK_{j,1} , \quad (1)$$

where 1 signifies material 1 (in this case the metal), j is phonon polarization, \hbar is the reduced Plank constant, ω is phonon frequency, K is phonon wave vector, ζ^{1-2} is the transmission coefficient of phonons crossing from material 1 to 2, v is the phonon group velocity, n_0 is the Bose-Einstein distribution of phonons, and T is temperature. This equation can be rewritten as an integral over ω by substituting $\frac{d\omega_{j,1}}{dK_{j,1}}$ for $v_{j,1}(K_{j,1})$ and canceling $dK_{j,1}$ as follows :

$$G_p = \frac{1}{8\pi^2} \sum_j \int_{\omega_{j,1}} \hbar \omega_{j,1} K_{j,1}^2 \zeta^{1-2} \frac{\partial n_0}{\partial T} d\omega_{j,1} = \sum_j \int_{\omega_{j,1}} g_{j,1}(\omega) d\omega_{j,1} , \quad (2)$$

where $g_{j,1}$ is a spectral thermal interface conductance per unit ω .

The ζ^{1-2} in eq. (1) and eq. (2) needs to be defined for complete calculation of G_p . The DMM assumes diffuse elastic scattering at the interface for all incident phonons as an accepted approach to estimate ζ^{1-2} . Notably, the DMM ignores details of the interface and bases its prediction of ζ^{1-2} entirely on the bulk phonon properties in materials 1 and 2. The elastic scattering assumption and detailed balance lead to an expression for ζ^{1-2} as follows⁴⁶:

$$\zeta^{1-2}(\omega) = \frac{\sum_j (K_{j,2}(\omega))^2}{\sum_j (K_{j,1}(\omega))^2 + \sum_j (K_{j,2}(\omega))^2} . \quad (3)$$

It is well known that the use of Debye dispersion overestimates contributions of Brillouin zone edge phonons to G_p . Therefore, we instead used the real dispersion relationships to calculate ζ^{1-2} and G_p .^{45,47} Dispersion relationships for our materials (Au, Cu, Cr and Al₂O₃) were formulated by fitting a fourth-order polynomial to experimentally obtained ω values as a function of K for each acoustic polarization branch.^{26,48-51} The phonon propagation directions in the real dispersion relationships of our materials were chosen to be Γ -L [111] in Cu and Au, Γ -N [110] in Cr, and Γ -Z [0001] for Al₂O₃. These directions were chosen based on the Al₂O₃ substrate normal direction and on the expected growth texture in each of the films, which differ because Cr is body centered cubic while Au and Cu are face centered cubic.⁵²⁻⁵⁶

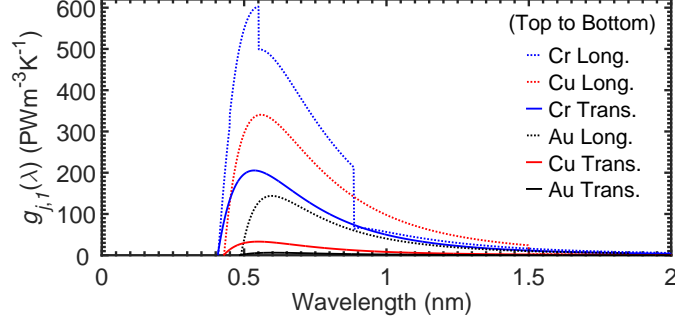


Figure 3: The interface thermal conductance per unit wavelength, $g_{j,1}(\lambda)$, for each polarization branch in our metallic materials calculated using eq.(5).

To predict G_p as a function of adhesion layer thickness we assume that only phonons of wavelength (λ) less than the adhesion layer thickness (t) can exist in the layers. Notably, this assumption disregards changes to the phonon dispersion that may exist in very thin adhesion layers. The assumption that λ_{\max} equals t leads us to consider the accumulation of G_p with λ . A recent study by Cheaito et al.⁵⁷ described the thermal interface conductance accumulation function as a function of ω as follows:

$$G_{p,\text{accum.}}^{1 \rightarrow 2}(\omega_a) = \sum_j \int_0^{\omega_a} g_{j,1}(\omega) d\omega_{j,1} \quad (4)$$

The $g_{j,1}(\omega)$ can be converted to $g_{j,1}(\lambda)$ through a change of variables as follows:

$$G_{p,\text{accum.}}^{1 \rightarrow 2}(\lambda_a) = \sum_j \int_{\lambda_{\min}}^{\lambda_a} -g_{j,1}(\omega) \frac{d\omega_{j,1}}{d\lambda_{j,1}} d\lambda_{j,1} = \sum_j \int_{\lambda_{\min}}^{\lambda_a} g_{j,1}(\lambda) d\lambda_{j,1}, \quad (5)$$

where λ_{\min} is the shortest phonon wavelength defined by K_{\max} at the Brillouin zone edge. The term $\frac{d\omega}{d\lambda}$ can be analytically evaluated using the relationship between ω and K that is established in the dispersion relationships and the definition of $K = \frac{2\pi}{\lambda}$. Fig. 3 shows $g_{j,1}(\lambda)$ for each polarization branch in our metals. The contributions from short λ are the largest because the phonon density of states is highest for short λ — an effect that overpowers their lower relative $v_{j,1}(K_{j,1})$. Discontinuities in $g_{j,1}(\lambda)$ shown in Fig. 3 result from discontinuities in $\zeta^{1 \rightarrow 2}$ caused by the differing frequency ranges spanned by each polarization (e.g., transmission of longitudinal modes is higher for frequencies above that spanned by transverse modes because there are less options for reflection).

We further assume that phonons with λ greater than the adhesion layer thickness come

from the Au layer directly. The physical interpretation of this assumption is that phonons with wavelengths longer than the adhesion layer transmit through it, as if it were transparent. While this assumption is not rigorous, there are many complications to creating a more rigorous model. In particular, the diversity of bonding due to the juxtaposition of three materials would influence the local vibrational states in a nontrivial way. Our approach is a first order approximation that sheds light on the experimental result and even agrees reasonably, yet has clear shortcomings, that are beyond the scope of this study. Therefore, $G(t)$ can be expressed as :

$$G_p(t) = G_{p,accum.}^{AL \rightarrow Al_2O_3}(t) + (G_{p,Au \rightarrow Al_2O_3} - G_{p,accum.}^{Au \rightarrow Al_2O_3}(t)) \quad (6)$$

where $G_{p,accum.}^{AL \rightarrow Al_2O_3}$ is the accumulated G_p as a function of adhesion layer (AL) thickness, $G_{p,Au \rightarrow Al_2O_3}$ is the maximum value of $G_{p,accum.}^{Au \rightarrow Al_2O_3}(t)$, and $G_p(t)$ is the accumulated G_p as a function of the adhesion layer thickness.

The calculated $G_p(t)$ at 300 K is plotted in Fig. 2(b). A plateau in the predicted $G_p(t)$ occurs for adhesion layer thicknesses greater than ~ 2 nm. The maximum predicted values are $180 \text{ MW m}^{-2} \text{ K}^{-1}$ and $400 \text{ MW m}^{-2} \text{ K}^{-1}$, which are in reasonable agreement with our measured values of the thickest Cu and Cr films. The AMM, on the other hand, highly overestimated our results, yielding $\sim 300 \text{ MW/m}^{-2} \text{ K}^{-1}$, $\sim 540 \text{ MW/m}^{-2} \text{ K}^{-1}$, and $\sim 900 \text{ MW/m}^{-2} \text{ K}^{-1}$ for Al_2O_3 interfaces with Au, Cu and Cr. Notably, the predictions of G_p exclude G_{e-p} while it is included in the measured G as previously discussed. The fact that the DMM captures our observed accumulation with thickness suggests that it may be a reasonable predictive tool — even for very thin adhesion layers. An alternative DMM interpretation may be that $\lambda_{max} = 2t$, which would cause faster accumulation with thickness. Given the uncertainty of our thickness measurement, we cannot use this dataset to confirm whether adhesive effects at the interface play a significant role for thicknesses less than the minimum phonon wavelength.²⁵ Excluding this range, the difference between the DMM and experiment is not great enough to require the invocation of additional interfacial mechanisms at work in determining phonon transmission beyond alignment of the density of states of the two interfaced materials.

IV. CONCLUSIONS

We measured a significant increase in G at the metal-dielectric Au- Al_2O_3 interface as a function of Cu and Cr adhesion layer thickness inserted between Au and Al_2O_3 . Both Cu and Cr showed a saturation of G ($390 \pm 70 \text{ MW m}^{-2}\text{K}^{-1}$ in Cr and $180 \pm 20 \text{ MW m}^{-2}\text{K}^{-1}$ in Cu) once the layer thickness exceeded 5 nm. From a plasmonic technological perspective having a very thin adhesion layer minimizes disruption of the optical properties that are critical to the plasmonic performance. The experimentally observed G values were compared with predictions, where the transmission coefficients were obtained using the DMM with real dispersion relationships. Both calculated and experimental values agreed well suggesting that phonon alignment is indeed a dominant mechanism in increasing G with very thin adhesion layers, rather than the enhancement of electron-phonon coupling on the metal side of the interface. Notably, the use of metal adhesion layers at the metal-dielectric interface also generates a new metal-metal interface that was not herein a focal point. Because electrons transmit efficiently between metal layers, this metal-metal interface has very high thermal conductance, and therein plays little role in the total G . Dielectric adhesion layers would instead introduce two phonon dominated interfaces, though could still be beneficial for adhesion and bridging of dissimilar phonon states.

ACKNOWLEDGMENTS

We acknowledge financial support from the National Science Foundation (NSF CBET 1403447) and the Data Storage Systems Center (DSSC) at Carnegie Mellon University as well as helpful discussions with John C. Duda from Seagate Technology.

* jonmalen@andrew.cmu.edu

¹ C. L. Kane and E. J. Mele, “Quantum Spin Hall Effect in Graphene,” *Physical Review Letters* **95**, 226801 (2005).

² Haijun Zhang, Chao-Xing Liu, Xiao-Liang Qi, Xi Dai, Zhong Fang, and Shou-Cheng Zhang, “Topological insulators in Bi_2Se_3 , Bi_2Te_3 and Sb_2Te_3 with a single Dirac cone on the surface,” *Nature Physics* **5**, 438–442 (2009).

- ³ M. Z. Hasan and C. L. Kane, “*Colloquium*: Topological insulators,” *Reviews of Modern Physics* **82**, 3045–3067 (2010).
- ⁴ Vincent Sacksteder, Tomi Ohtsuki, and Koji Kobayashi, “Modification and Control of Topological Insulator Surface States Using Surface Disorder,” *Physical Review Applied* **3**, 064006 (2015).
- ⁵ W. A. Challener, Chubing Peng, A. V. Itagi, D. Karns, Wei Peng, Yingguo Peng, XiaoMin Yang, Xiaobin Zhu, N. J. Gokemeijer, Y.-T. Hsia, G. Ju, Robert E. Rottmayer, Michael A. Seigler, and E. C. Gage, “Heat-assisted magnetic recording by a near-field transducer with efficient optical energy transfer,” *Nature Photonics* **3**, 220–224 (2009).
- ⁶ Zhi-Min Yuan, Jianzhong Shi, Chun Lian Ong, P.S. Alexopoulos, Chunling Du, Anmin Kong, Shiming Ang, B. Santoso, Siang Huei Leong, Kheong Sann Chan, Yibin Ng, Kui Cai, J. Tsai, Hanxiang Ng, and Hang Khume Tan, “Dedicated Servo Recording System and Performance Evaluation,” *IEEE Transactions on Magnetics* **51**, 1–7 (2015).
- ⁷ L. Huang, B. Stipe, M. Staffaroni, J.-Y. Juang, T. Hirano, E. Schreck, and F.-Y. Huang, “HAMR Thermal Modeling Including Media Hot Spot,” *IEEE Transactions on Magnetics* **49**, 2565–2568 (2013).
- ⁸ E. T. Swartz and R. O. Pohl, “Thermal boundary resistance,” *Reviews of Modern Physics* **61**, 605–668 (1989).
- ⁹ Yibin Xu, Haitao Wang, Yoshihisa Tanaka, Masato Shimono, and Masayoshi Yamazaki, “Measurement of Interfacial Thermal Resistance by Periodic Heating and a Thermo-Reflectance Technique,” *Materials Transactions* **48**, 148–150 (2007).
- ¹⁰ R. J. Stoner and H. J. Maris, “Kapitza conductance and heat flow between solids at temperatures from 50 to 300 K,” *Physical Review B* **48**, 16373–16387 (1993).
- ¹¹ Robert J. Stevens, Andrew N. Smith, and Pamela M. Norris, “Measurement of Thermal Boundary Conductance of a Series of Metal-Dielectric Interfaces by the Transient Thermoreflectance Technique,” *Journal of Heat Transfer* **127**, 315–322 (2005).
- ¹² Kimberlee C. Collins, Alexei A. Maznev, John Cuffe, Keith A. Nelson, and Gang Chen, “Examining thermal transport through a frequency-domain representation of time-domain thermoreflectance data,” *Review of Scientific Instruments* **85**, 124903 (2014).
- ¹³ J. Lombard, F. Detcheverry, and S. Merabia, “Influence of the electron-phonon interfacial conductance on the thermal transport at metal/dielectric interfaces,” *Journal of Physics: Condensed Matter* **27**, 015007 (2015).

- ¹⁴ Yan Wang, Xiulin Ruan, and Ajit K. Roy, “Two-temperature nonequilibrium molecular dynamics simulation of thermal transport across metal-nonmetal interfaces,” *Physical Review B* **85**, 205311 (2012).
- ¹⁵ Arun Majumdar and Pramod Reddy, “Role of electron-phonon coupling in thermal conductance of metal-nonmetal interfaces,” *Applied Physics Letters* **84**, 4768–4770 (2004).
- ¹⁶ R. E. Jones, J. C. Duda, X. W. Zhou, C. J. Kimmer, and P. E. Hopkins, “Investigation of size and electronic effects on Kapitza conductance with non-equilibrium molecular dynamics,” *Applied Physics Letters* **102**, 183119 (2013).
- ¹⁷ Patrick E. Hopkins, John C. Duda, Bryan Kaehr, Xiao Wang Zhou, C.-Y. Peter Yang, and Reese E. Jones, “Ultrafast and steady-state laser heating effects on electron relaxation and phonon coupling mechanisms in thin gold films,” *Applied Physics Letters* **103**, 211910 (2013).
- ¹⁸ Piyush Singh, Myunghoon Seong, and Sanjiv Sinha, “Detailed consideration of the electron-phonon thermal conductance at metal-dielectric interfaces,” *Applied Physics Letters* **102**, 181906 (2013).
- ¹⁹ R. B. Wilson, Joseph P. Feser, Gregory T. Hohensee, and David G. Cahill, “Two-channel model for nonequilibrium thermal transport in pump-probe experiments,” *Physical Review B* **88**, 144305 (2013).
- ²⁰ Edward Dechaumphai, Dylan Lu, Jimmy J. Kan, Jaeyun Moon, Eric E. Fullerton, Zhaowei Liu, and Renkun Chen, “Ultralow Thermal Conductivity of Multilayers with Highly Dissimilar Debye Temperatures,” *Nano Letters* **14**, 2448–2455 (2014).
- ²¹ A. V. Sergeev, “Electronic Kapitza conductance due to inelastic electron-boundary scattering,” *Physical Review B* **58**, R10199–R10202 (1998).
- ²² Wei Wang and David G. Cahill, “Limits to Thermal Transport in Nanoscale Metal Bilayers due to Weak Electron-Phonon Coupling in Au and Cu,” *Physical Review Letters* **109**, 175503 (2012).
- ²³ I. M. Lifshits M. I. Kaganov, “Relaxation between electrons and crystalline lattice. *Sov Phys JETP* 4:173,” *Soviet Physics, JETP* **31** (1957).
- ²⁴ J. C. Duda, C.-Y. P. Yang, B. M. Foley, R. Cheaito, D. L. Medlin, R. E. Jones, and P. E. Hopkins, “Influence of interfacial properties on thermal transport at gold:silicon contacts,” *Applied Physics Letters* **102**, 081902 (2013).
- ²⁵ Timothy S. English, John C. Duda, Justin L. Smoyer, Donald A. Jordan, Pamela M. Norris, and Leonid V. Zhigilei, “Enhancing and tuning phonon transport at vibrationally mismatched solid-

- solid interfaces,” *Physical Review B* **85**, 035438 (2012).
- ²⁶ See Supplemental Material at [URL] for surface characteristics of our grown films, uncertainties in the X-ray reflectivity (XRR) measurements of thickness, and our formulated dispersion relationships.
- ²⁷ Wee-Liat Ong, Sara M. Rupich, Dmitri V. Talapin, Alan J. H. McGaughey, and Jonathan A. Malen, “Surface chemistry mediates thermal transport in three-dimensional nanocrystal arrays,” *Nature Materials* **12**, 410–415 (2013).
- ²⁸ Jonathan A. Malen, Kanhayalal Baheti, Tao Tong, Yang Zhao, Janice A. Hudgings, and Arun Majumdar, “Optical Measurement of Thermal Conductivity Using Fiber Aligned Frequency Domain Thermoreflectance,” *Journal of Heat Transfer* **133**, 081601–081601 (2011).
- ²⁹ Aaron J. Schmidt, Xiaoyuan Chen, and Gang Chen, “Pulse accumulation, radial heat conduction, and anisotropic thermal conductivity in pump-probe transient thermoreflectance,” *Review of Scientific Instruments* **79**, 114902 (2008).
- ³⁰ David G. Cahill, “Analysis of heat flow in layered structures for time-domain thermoreflectance,” *Review of Scientific Instruments* **75**, 5119–5122 (2004).
- ³¹ A. Gäßel, F. Hemberger, S. Vidi, and H.-P. Ebert, “A New Method for the Determination of the Specific Heat Capacity Using Laser-Flash Calorimetry Down to 77k,” *International Journal of Thermophysics* **34**, 883–893 (2012).
- ³² R. H. Beaumont, H. Chihara, and J. A. Morrison, “An anomaly in the heat capacity of chromium at 38Å5Åř,” *Philosophical Magazine* **5**, 188–191 (1960).
- ³³ Fran Cverna, *ASM Ready Reference: Thermal properties of metals* (ASM International, 2002).
- ³⁴ Keith T. Regner, Daniel P. Sellan, Zonghui Su, Cristina H. Amon, Alan J. H. McGaughey, and Jonathan A. Malen, “Broadband phonon mean free path contributions to thermal conductivity measured using frequency domain thermoreflectance,” *Nature Communications* **4**, 1640 (2013).
- ³⁵ Mark D. Losego, Martha E. Grady, Nancy R. Sottos, David G. Cahill, and Paul V. Braun, “Effects of chemical bonding on heat transport across interfaces,” *Nature Materials* **11**, 502–506 (2012).
- ³⁶ Bryan C. Gundrum, David G. Cahill, and Robert S. Averback, “Thermal conductance of metal-metal interfaces,” *Physical Review B* **72**, 245426 (2005).
- ³⁷ JP Moore, RK Williams, and RS Graves, “Thermal conductivity, electrical resistivity, and seebeck coefficient of high-purity chromium from 280 to 1000 k,” *Journal of Applied Physics* **48**, 610–617 (1977).

- ³⁸ SD Brorson, A Kazeroonian, JS Moodera, DW Face, TK Cheng, EP Ippen, MS Dresselhaus, and G Dresselhaus, “Femtosecond room-temperature measurement of the electron-phonon coupling constant γ in metallic superconductors,” *Physical Review Letters* **64**, 2172 (1990).
- ³⁹ HE Elsayed-Ali, TB Norris, MA Pessot, and GA Mourou, “Time-resolved observation of electron-phonon relaxation in copper,” *Physical Review Letters* **58**, 1212 (1987).
- ⁴⁰ REB Makinson, “The thermal conductivity of metals,” in *Mathematical Proceedings of the Cambridge Philosophical Society*, Vol. 34 (Cambridge Univ Press, 1938) pp. 474–497.
- ⁴¹ Alexander A Balandin, “Thermal properties of graphene and nanostructured carbon materials,” *Nature materials* **10**, 569–581 (2011).
- ⁴² Yongjie Hu, Lingping Zeng, Austin J Minnich, Mildred S Dresselhaus, and Gang Chen, “Spectral mapping of thermal conductivity through nanoscale ballistic transport,” *Nature nanotechnology* (2015).
- ⁴³ Robert J. Stevens, Pamela M. Norris, and Leonid V. Zhigilei, “Molecular Dynamics Study of Thermal Boundary Resistance: Evidence of Strong Inelastic Scattering Transport Channels,” , 37–46 (2004).
- ⁴⁴ M. Kazan, “Interpolation between the acoustic mismatch model and the diffuse mismatch model for the interface thermal conductance: Application to inn/gan superlattice,” *Journal of Heat Transfer* **133**, 112401–112401 (2011).
- ⁴⁵ John C. Duda, Thomas E. Beechem, Justin L. Smoyer, Pamela M. Norris, and Patrick E. Hopkins, “Role of dispersion on phononic thermal boundary conductance,” *Journal of Applied Physics* **108**, 073515 (2010).
- ⁴⁶ John C. Duda, Justin L. Smoyer, Pamela M. Norris, and Patrick E. Hopkins, “Extension of the diffuse mismatch model for thermal boundary conductance between isotropic and anisotropic materials,” *Applied Physics Letters* **95**, 031912 (2009).
- ⁴⁷ Pramod Reddy, Kenneth Castelino, and Arun Majumdar, “Diffuse mismatch model of thermal boundary conductance using exact phonon dispersion,” *Applied Physics Letters* **87**, 211908 (2005).
- ⁴⁸ J. W. Lynn, H. G. Smith, and R. M. Nicklow, “Lattice Dynamics of Gold,” *Physical Review B* **8**, 3493–3499 (1973).
- ⁴⁹ H Schober, D Strauch, and B Dorner, “Lattice dynamics of sapphire (al₂o₃),” *Zeitschrift für Physik B Condensed Matter* **92**, 273–283 (1993).
- ⁵⁰ Ruqing Xu, Hawoong Hong, Paul Zschack, and T.-C. Chiang, “Direct Mapping of Phonon Dispersion Relations in Copper by Momentum-Resolved X-Ray Calorimetry,” *Physical Review Letters* **101**,

085504 (2008).

- ⁵¹ L. D. Muhlestein W. M. Shaw, “Investigation of the Phonon Dispersion Relations of Chromium by Inelastic Neutron Scattering,” *Phys. Rev. B* **4** (1971), 10.1103/PhysRevB.4.969.
- ⁵² Takeo Sasaki, Katsuyuki Matsunaga, Hiromichi Ohta, Hideo Hosono, Takahisa Yamamoto, and Yuichi Ikuhara, “Atomic and electronic structures of Cu/ α -Al₂O₃ interfaces prepared by pulsed-laser deposition,” *Science and Technology of Advanced Materials* **4**, 575–584 (2003).
- ⁵³ Zoe Boekelheide and F Hellman, “Cr (110) texture induced by epitaxy on Al₂O₃ (0001) substrates: Preferential grain growth in the < 001 > direction,” *Applied Physics Letters* **102**, 141601 (2013).
- ⁵⁴ S Tsukimoto, F Phillipp, and T Wagner, “Texture of mbe grown Cr films on α -Al₂O₃ (0001): the occurrence of nishiyama-wassermann (nw) and kurdjumov-sachs (ks) related orientation relationships,” *Journal of the European Ceramic Society* **23**, 2947–2954 (2003).
- ⁵⁵ Christine Marie Montesa, Naoya Shibata, Tetsuya Tohei, Kazuhiro Akiyama, Yoshirou Kuromitsu, and Yuichi Ikuhara, “Application of coincidence of reciprocal lattice point model to metal/sapphire hetero interfaces,” *Materials Science and Engineering: B 3rd International Conference on Science and Technology of Advanced Ceramics*, **173**, 234–238 (2010).
- ⁵⁶ Hila Sadan and Wayne D Kaplan, “Au–sapphire (0001) solid–solid interfacial energy,” *Journal of materials science* **41**, 5099–5107 (2006).
- ⁵⁷ Ramez Cheaito, John T. Gaskins, Matthew E. Caplan, Brian F. Donovan, Brian M. Foley, Ashutosh Giri, John C. Duda, Chester J. Szwejkowski, Costel Constantin, Harlan J. Brown-Shaklee, Jon E. Ihlefeld, and Patrick E. Hopkins, “Thermal boundary conductance accumulation and interfacial phonon transmission: Measurements and theory,” *Phys. Rev. B* **91**, 035432 (2015).